Airframe Optimization

Ryan Howell

December 3, 2024

1 Introduction

Throughout this course, I have read Julia function documentation and several textbook chapters to learn more about the design and analysis of airframes. Initially, I learned about the panel method and, through experimenting with Xfoil.jl, observed the aerodynamic effects of airfoil design. Building on this foundation, I explored the aerodynamic effects of wing shape, angle of attack, and tail volume ratios using Vortex.jl. Subsequently, I optimized the design of a wing for lift varying several parameters using Vortex.jl. Finally, I optimized several parameters of an entire airframe for range. These results, supported by theoretical principles, will be detailed in the following report.

2 XFOIL.jl and Airfoil Exploration

Through the airfoil exploration using XFOIL.jl I gained a foundational understanding of airfoil aerodynamics, NACA airfoil standardization, and the panel method's approach and assumptions, which are crucial for interpreting Xfoil functions. Airfoils experience lift and drag forces, influenced by factors such as the angle of attack, Reynolds number, and airfoil shape, with the chord line serving as a reference. NACA airfoils are standardized using a four-digit code that represents the maximum camber, its position from the leading edge, and the maximum thickness, all as percentages of the chord length, ensuring consistent airfoil shapes for experiments. The panel method involves dividing the airfoil into linear panels to calculate lift, drag, and moment coefficients, relying on assumptions like zero induced velocity at a distance, tangential flow to the airfoil, and the Kutta condition for continuous flow off the trailing edge, which are essential for deriving the method's equations. These allowed us to explore several performance measures of various airfoils.

2.1 Effect of the Angle of Attack on an Airfoil

This section discusses the impact of the angle of attack on airfoil behavior, using data from Xfoil to illustrate changes in lift, drag, and moment coefficients. Figure 1 shows that the lift coefficient increases with the angle of attack until it surpasses ten degrees, where it drops sharply, indicating the stall angle. To maintain lift, the angle of attack must remain below this stall angle. Similarly, the drag coefficient gradually increases with the angle of attack but spikes sharply past ten degrees, see Figure 2, correlating with the stall angle. This sharp increase in drag, combined with the drop in lift, causes the plane to stall. Therefore, optimizing the angle of attack involves balancing lift and drag to avoid stalling. The moment coefficient remains relatively stable around a small negative value, as shown in 3.

2.1.1 Published Data Comparison

Exploring how the panel method results from Xfoil compared to published Xfoil data and experimental data for the same airfoil, a relatively close match is seen. By comparing it to published data from Xfoil programs we can verify the functions are working as expected, while other comparisons help us evaluate the effectiveness of the panel method in general. In the experimental plots there are slight differences from the Xfoil data, but the overall trends are the same. Looking at Xfoil data generated by others for 6412 and 0012 NACA airfoils using a Reynolds number of 1 million, we can verify if our
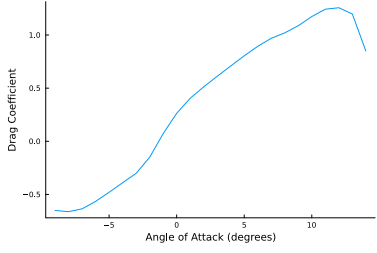
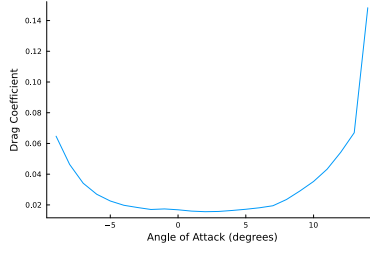Figure 1: Lift of a NACA 2412 airfoil in flow with a Reynolds number of 100 thousand

Figure 2: Drag of a NACA 2412 airfoil in flow with a Reynolds number of 100 thousand
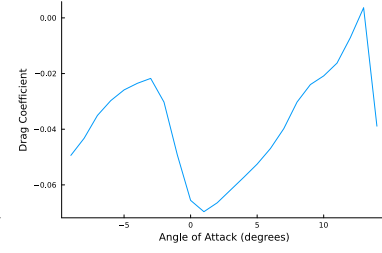

Figure 3: Moment of a NACA 2412 Airfoil in Flow with a Reynolds Number of 100000

Xfoil code is providing realistic results [Aer24]. Our moment coefficient calculations match as shown in Figures 4.

I further verified this simulated data by comparing it to experimental data collected by NASA [AB94] in the 90's testing airfoils in a wind tunnel. Examining Figure 5 showing that the experimental data is a near perfect match for the predicted lift coefficient. However, when comparing the drag coefficients, 6, we see that the generated Xfoil plot is a close match but not quite exact. The Xfoil method aligns well with real data, CFD simulations, and other Xfoil programs. Overall, the panel method is accurate in estimating the lift, drag, and moment coefficients of a NACA airfoil for a given angle of attack and Reynolds number.
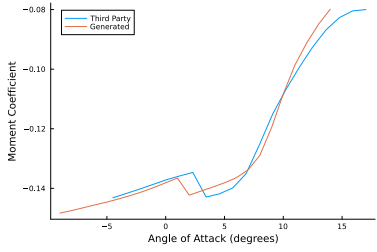

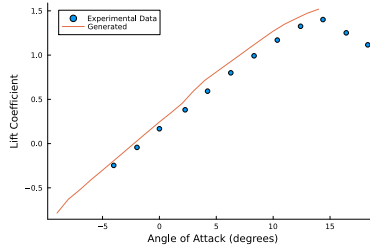Figure 4: Moment coefficient third party Xfoil data comparison, NACA 6412

Figure 5: Lift coefficient comparison with experimental data, NACA 2412
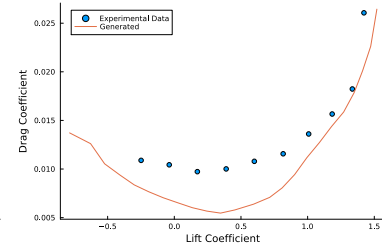

Figure 6: Lift to drag ratio comparison with experimental data, NACA 2412

2.1.2 Effect of Airfoil Shape

The shape of the airfoil significantly affects fluid flow impacting the lift, drag, and moment coefficients. Camber, the curve or asymmetry of the wing, is one way to manipulate airfoil shape. It is the maximum distance between the chord line and a line equidistant between the upper and lower surfaces. For a symmetrical airfoil the camber is 0. Increased camber results in more lift at a given angle of attack even if the lift curve slope remains constant, see 8. This likewise shifts the lift to drag ratio up, see Figure 7.
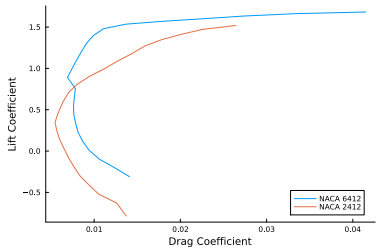

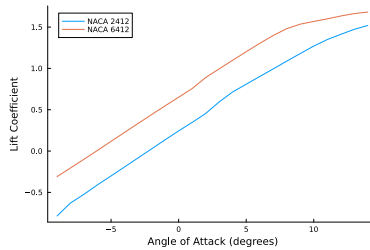Figure 7: Effect of Camber on the lift to drag ratio

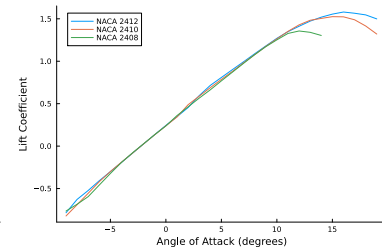Figure 8: Effect of Camber on Lift

Figure 9: Effect of thickness on lift

2.1.3 Thickness

Thickness, the maximum distance between the upper and lower surfaces of the airfoil perpendicular to the chord line, is another way we can manipulate the shape of the airfoil. Thinner airfoils stall earlier as shown in 9. This likewise results in a lower lift to drag ratios.

3 Analysis of a Wing

Manipulating wing geometry, such as sweep, twist, chord, and dihedral angle, alters aerodynamics and reference area, with downwash being an unavoidable effect that can be mitigated by expanding the span or using closed wings. Vortices, induced by wing geometry, can be mapped and simplified into a horseshoe vortex, forming the basis of the Vortex Lattice method, which relates lift coefficient to circulation and extends into three dimensions for the aerodynamic analysis of thin wings. Compressible flow becomes significant at high speeds, where fluid compression leads to shock waves and new drag types, influencing high-speed aircraft design and necessitating considerations like thin-airfoil theory and mach cones. The shape of the wing determines many factors such as chord lengths and reference areas, and the relationship of these and other variables creates different lift coefficients as the shape of the wing changes. I examine the effect of these wing shapes along with how they affect wing efficiency, which will then be analyzed in the frame of how the vortex lattice approach analyzes these results given different lattice structures, presenting graphics produced through the properties obtained via the vortex lattice method.

3.1 Elliptic Wing

An elliptic wing is a half ellipse for a singular wing or a full ellipse when both wings are put together. To analyze this wing I created a function that creates the wing, leading edge points, and chord lengths given the root chord and span of the wing.

The first study was of the effect of adding more vertical sections to the wing on the shape and behavior of the lift distribution. As shown in Figure 10, when you add sections, the lift distribution seems to approach this flattened elliptic shape. This is true to a point until the increasingly shortened changes and small chord lengths in vortex lattice creates abnormal and unrealistic behavior, seen as spikes in lift as shown below in Figure 10.
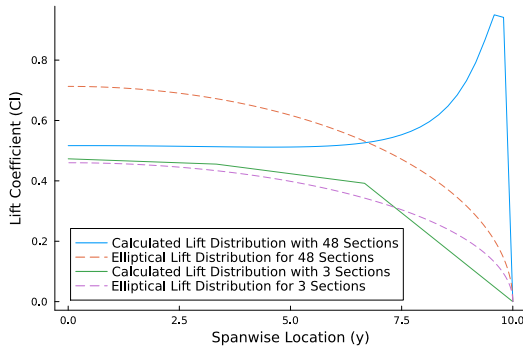

Figure 10: Efficiency comparison of elliptic wing with increased number of sections
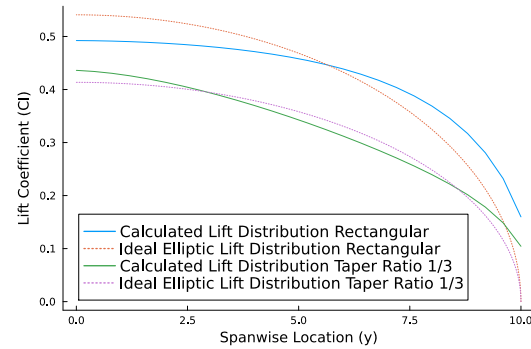
Figure 11: Polygonal wing shapes lift distributions

3.2 Other Wing Shapes

I also created a function similar to the elliptic wing generator that takes in a tip chord in addition to the previously described variables to produce the necessary information to analyze a quadrilateral wing profile. This allowed me to generate rectangular and tapered wings. The lift profiles of these wings do not align perfectly with an ideal elliptic lift distribution as shown in Figure 11. For this particular wing taper it approaches the efficiency of an elliptical wing, showing the ability of a tapered wing to optimize the lift distribution of a wing.

3.3 Tail Volume Ratios and Stability Derivatives

The tail of a plane through the use of the rudder and elevator, determine the pitch and yaw of a plane. The overall shape of each part of the tail, in turn, affects the stability of the plane in these directions. A grid of the stability derivatives related to pitch and yaw showing the effect of increasing the horizontal and vertical tail volume ratios is attached as Figure 4 in Appendix A. These results, however, include various less interesting results. Tables 1 and 2 focus on the more interesting variable changes caused by changing the horizontal and vertical tail volume ratios respectively.

3.3.1 Results

Table 4 in Appendix A extensively shows that the horizontal tail volume ratio has a nearly exclusive effect on the pitch stability-related derivatives. The effect of the horizontal tail volume ratio is highlighted in Figure 1. While the vertical tail volume ratio has a similar effect on the yaw stability-related derivatives, its effect is highlighted in Figure 2. Examining these charts we see that changing the horizontal tail volume ratio greatly affects the stability derivatives related to angle of attack and pitch rate. Similarly, the vertical tail volume ratio greatly affects the stability derivatives related to the yaw angle and yaw rate.

Table 1: Effect of horizontal tail volume on pitch stability derivatives

		Stability Derivatives	
		α	q
	0.875	-1.2	-22.62
Vh	3.0625	-6.57	-296.70
	5.25	-11.88	-881.53

Table 2: Effect of vertical tail volume on yaw stability derivatives

		Stability Derivatives	
		β	r
	0.028	0.06	-0.05
Vv	0.168	0.39	-1.88
	0.308	0.72	-6.36

3.4 Effect of Angle of Attack on Lift

Similar to the lift of an airfoil, the lift of a wing increases with angle of attack, see Figure 12. However, unlike Xfoil.jl there is no clear stall that occurs in the tested range. This is likely due to the lack of viscous effects and subsequently separation, meaning the air is allowed to follow the airfoil closer and not separate. Without separation, there is no wake created that causes stall. This outlines one of the great limitations of the vortex lattice method. This means it will maintain a linear shape at high angles, which is an inaccurate assumption. Additionally, the vortex lattice method does not account for compressible flow, thick airfoils, or added complexities in the wake. This makes it limited in how it interprets sharp tips as seen with the elliptic wing lift distribution, see Figure 10. Despite these limitations, it remains a fairly accurate method for analyzing three-dimensional wings.
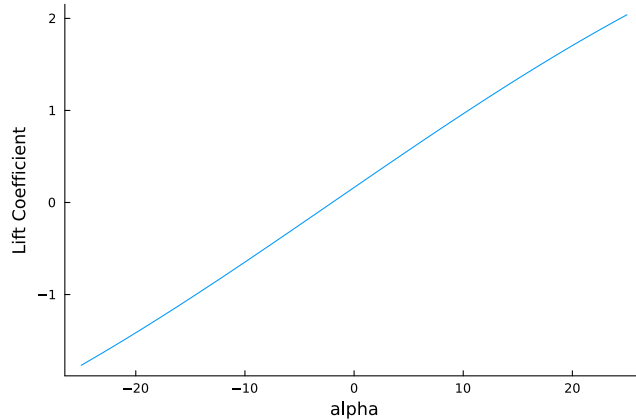

Figure 12: Effect of angle of attack on a whole wing

4 Optimization of a Wing

Building upon the wing analysis previously developed I then optimized various wing parameters including chord, twist, and angle of attack. The design process involves creating an initial design, evaluating, modifying, and iterating until an optimal design is achieved. Optimization algorithms can expedite this iterative process and often yield better solutions than manual calculations, but they require the problem to be formulated with constraints, an optimized parameter, and input variables. In SNOW.jl, constraints are set with upper and lower bounds, typically from negative infinity to zero, and defined within the function being optimized. Input parameters must also be defined with potential value ranges and an initial starting value. Once these are established, the minimize function can be used to optimize the design parameters for the given objective.

4.1 Optimized Airframe Design

Building on the airframe analysis from VortexLattice.jl, I used the Vortex Lattice method to set up an optimization problem to find the best wing shape.

4.1.1 Chord Distribution

The primary objective of this project was to optimize the chord distribution of a wing. This is accomplished by using the vortex lattice method to approximate the lift and drag of a wing in a function that was then optimized with the SNOW.jl wrapper. The objective was to minimize drag and maintain a required lift of 1.7 pounds, with constraints ensuring the wings retain a reasonable shape. These constraints include ensuring the chord length decreases across the span of the wing and limiting the variation between sections to a reasonable amount based on the number of sections. This approach maintains a realistic wing that meets the operating conditions for the plane while reducing the drag on the wing, or the required thrust. Due to the discussed limitations of Vortex Lattice as you optimize wing chords they don't go towards a perfect ellipse to avoid creating a point at the end of the wing. They do however produce a nearly elliptic wing that gets an elliptical distribution.

4.1.2 Changing the Number of Sections

Changing the number of sections allowed for increased refinement, as seen by comparing Figures 13 and 14. This creates a more accurate representation of the optimized wing. However, too many sections significantly slow down the optimization without much added resolution. In the refined wing profile, the optimized planform area is very elliptical, with the main deviation at the tip where it ends abruptly flat. This design avoids the sharp increase in lift coefficient predicted by Vortex Lattice for wings with sharp tips, as discussed in the previous section.
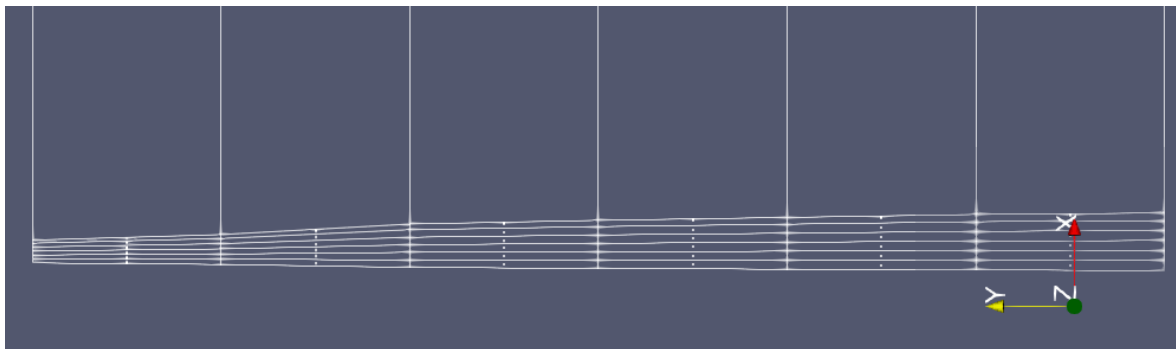

Figure 13: Optimized wing of 6 sections

4.1.3 The Effect of Constraints

Upon finding the optimal wing chord distribution, the restrictions on the change in chord from one section to the next were removed, leaving only the lift restriction. Using the previously found chord
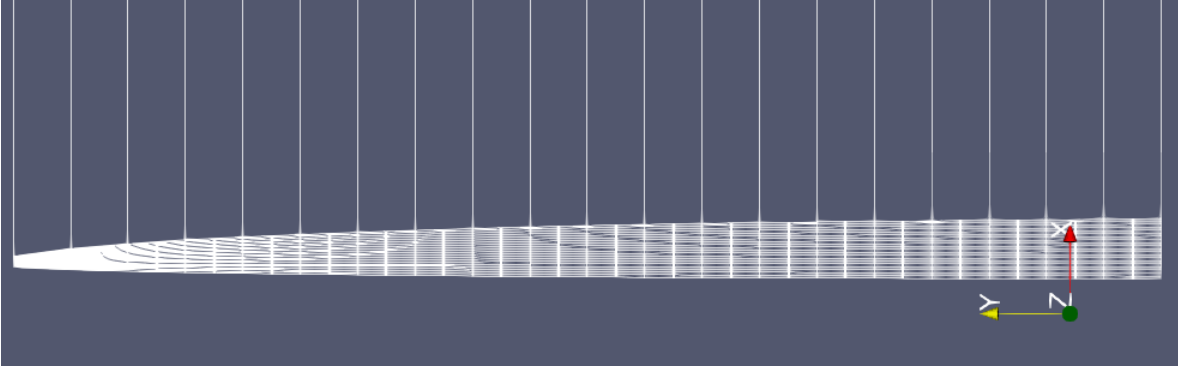
Figure 14: Optimized wing of 20 sections

distribution as the initial starting point, it converged to the same solution, shown in Figure 14, confirming its optimality and the appropriateness of those constraints. Then I varied the lift constraint by changing the weight of the aircraft, which had a drastic effect on the wing lift distribution. As seen in Figure 15, adding 4 pounds to the lift constraint caused the wing chords to lengthen. Increasing the lift constraint by a factor of five lengthened the chords even more, see Figure 16. This adjustment creates more lift while maintaining an elliptical shape. These larger wings resemble those of a Supermarine Spitfire, with the main difference being at the wingtips due to Vortex Lattice limitations as previously discussed. Increasing the plane's weight also increased the time needed to optimize the problem.
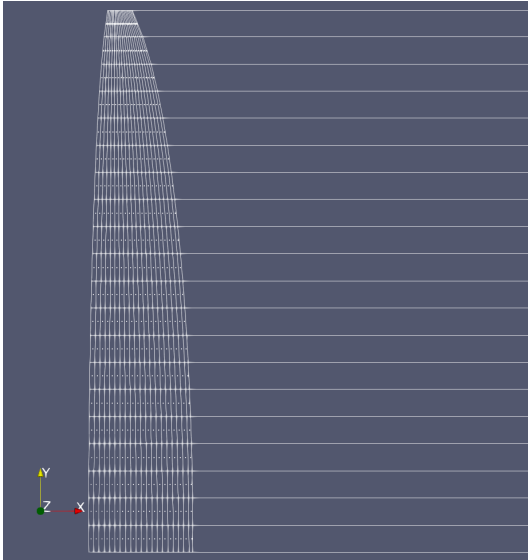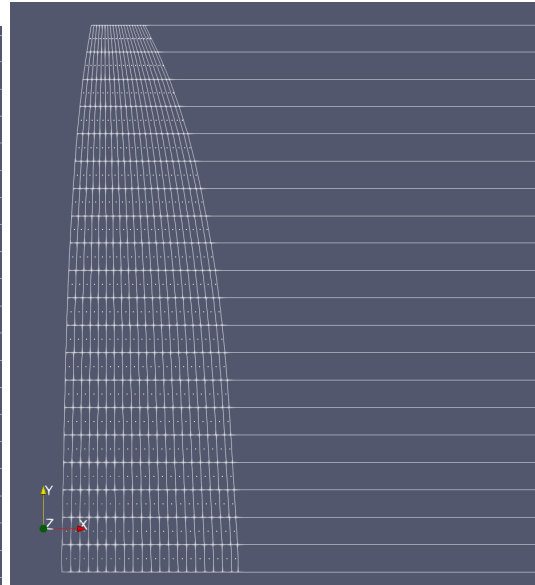

Figure 15: Optimized wing with 4 additional pounds

Figure 16: Optimized wing with 5 times the load

4.1.4 The Effect of the Tolerance

Increasing the lift constraint eventually leads to unsolvable scenarios, resulting in square wings or, through repeated iterations, partially square and elliptic wings but never converging to a solution. This can be reduced by increasing the tolerance, allowing the optimizer to run more quickly and reduce the precision of its search. Using the optimized chord distribution from previous iterations as an initial point, you can decrease the tolerance until an adequate tolerance is achieved. This approach allows for the wing to be optimized at a high tolerance for a more extreme scenario.

6

4.1.5 Optimizing Pitch Along with Chord Distribution

In this optimization problem, I had to pass in all the variables as one vector, which required separating the chords from the alpha value in the function. Once done, I could optimize the chord distribution and alpha angle separately. Interestingly, as shown in Figures 17 and 18, the root chord varied significantly less under increased loading when compared to Figures 14 and 16. The angle of attack was optimized to produce more lift while minimizing drag further. This led to a larger root chord at the normal lift requirement, 1.7 pounds, and a smaller root chord at 5 times that lift requirement. As noted in the image captions, the angle of attack increases with weight, which intuitively makes sense as a higher angle of attack produces more lift while adding some drag. The Vortex Lattice method introduces some inaccuracies at high alpha angles of attack as previously discussed, this was minimized through constraining the max alpha of around 15 degrees, which is near the stall angle of most airfoils.
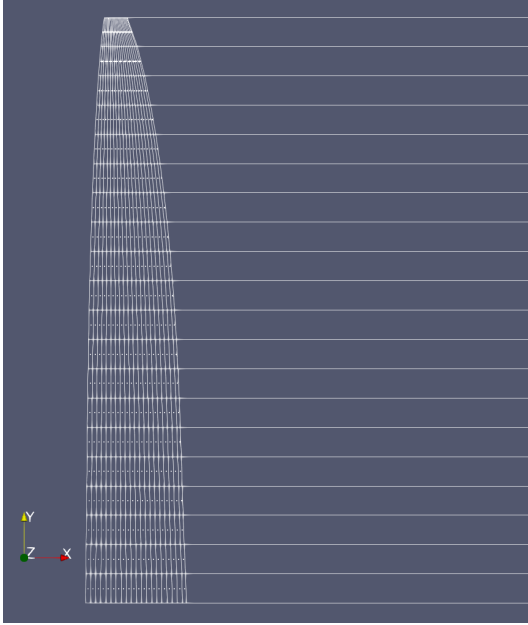

Figure 17: Optimized wing for base lift constraint and an optimized alpha of about 1.7 degrees
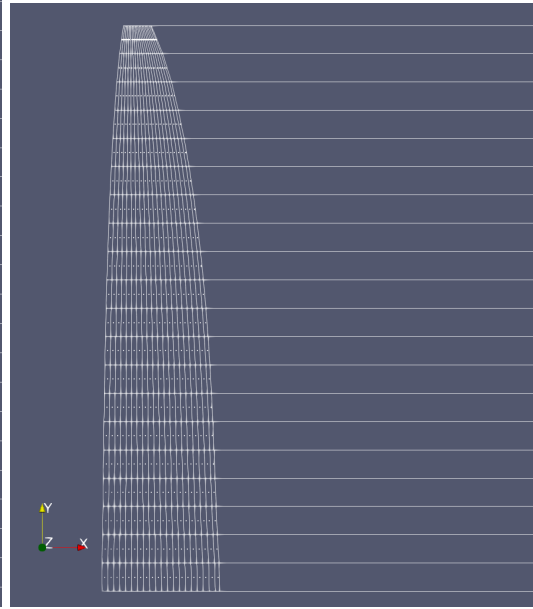
Figure 18: Optimized wing with 5 times the load and an optimized alpha of about 7.2 degrees

4.1.6 Varying Twist Angle

In this study, the chord distribution was kept constant across the wing span. The optimizer adjusted the theta vector to minimize drag while maintaining the required lift, allowing for negative twist. This optimization resulted in an elliptical lift distribution, as shown in Figures 19. The figures demonstrate that increasing the plane's weight causes the optimizer to generate more lift through additional twist while maintaining an elliptical lift distribution. This was done by increasing the twist of the wing. This indicates that wing twist can yield the same optimal lift distribution as an elliptical wing with other wing shapes.

5   Optimization of an Airframe for Range

Adjusting the previous problem to optimize an airframe for range included adding several more input values and changing the optimization objective. The objective was changed to minimize the force of drag over the flight speed multiplied by the square root of the force of lift. This is the approximate range equation holding constant the lift coefficient, specific fuel consumption, initial mass, and the final mass. This produced a slightly more complicated relationship than minimizing drag. I also included more design inputs to cover the design space of an entire airframe. Through iterative implementation
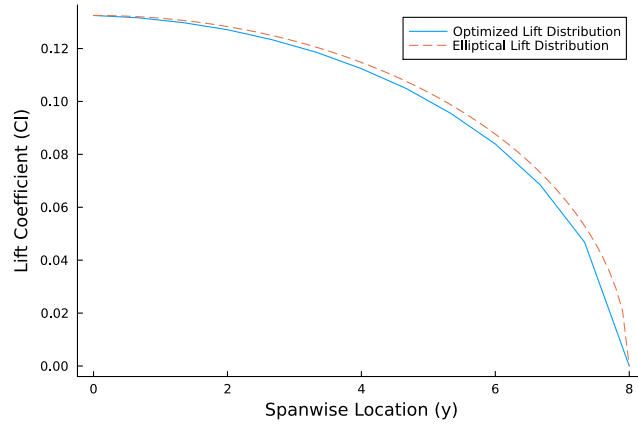
Figure 19: Lift distribution of a twisted, rectangular wing

I eventually optimized an airframe by varying the number of wing sections, the chord lengths of each section, dihedral of the wings, flight speed, position of the tail, the length of the vertical stabilizer, the length of the horizontal stabilizer, and then either the twist of each section or the span of the wing. As I iteratively added these variables one by one I would track the impact of the change to the speed and optimized parameter result to see how it affected the solution.

5.1   Dealing with Large Optimization Problems

To handle the shear number of optimized parameters required a faster optimization approach than the finite difference method previously used, such as forward differentiation. This required some adjustments in my problem setup and careful typing of variables to allow for a forward optimization. I also as mentioned above implemented each parameter one by one into the optimizer to ensure that it runs correctly. It also allowed me to see the benefit that optimizing for each parameter brought. The last parameters I implemented were the twist or span of the wing.

5.1.1   Constraints

The parameters were constrained to logical values. The range for each value in the input vector was held constant and then scaled accordingly to create sensible values. Twist and dihedral were limited to five degrees at each section for feasibility. Chords for the wing and each tail piece were likewise limited to five meters in length. The flight speed was limited to 10 m/s. The tail was limited to being 5 meters downstream from the leading edge of the wing, for certain optimization problems where the span and chord were both varied the tail was allowed to be 10 meters downstream to prevent solutions where the tail and wing overlapped. The airframe was also constrained to be stable by using the stability derivatives CYb and Cma. I also kept the weight constraint and the chords constraint that ensured the chords only tapered in from the root chord. The problem was set up to calculate the leading edge values from the chord values to create an aircraft with no sweep.

5.1.2   Multi-start

To ensure that the the resulting optimized parameters weren't just local minima I employed a multi start method to more extensively explore the design space. This method involved me setting up 10 different start points that had various patterns or randomized parameters as initial points to begin the optimization process. These start points took different amounts of time to converge to a local minima. Some of these minima matched those of other start points, resulting in a handful of potential answers. Examining these answers lead to adjusting my constraints to keep the optimized design within desirable parameters, such as chord or twist distribution. These were informed by manufacturability and other external concerns to performance.

8

To increase the accuracy of each of these answers the multi-start method was reemployed using the aforementioned answers as starting points with a higher tolerance. By using the end results as inputs and repeatedly tightening the tolerance till the local minima was well refined. The resulting optimized parameter for each of these local minima was compared to find the absolute minimum. Once identified this minimum can be used as a starting point for tweaking the optimization problem and setup. It also could serve as a point of comparison for adjusting the selected input parameters to see if giving the problem a broader design space would lead to a more optimal solution.

5.2 Results

Using the optimization of all the parameters outlined above and multi-start to find various local minima, four general wing patterns were found. One of these designs was eliminated as it resulted in a negative optimized goal exposing a weakness in the optimizer. The remaining three wing designs by incrementally tightening the tolerance eventually converged to a singular design whose parameters never varied more than a couple thousandths, aside from a slight .15 degree variation in twist at the tip. The optimized wing and chord distribution can be seen in Figure 20 and the whole plane is shown in Figure 21. A preliminary design the plane converges to before the tolerance is tightened is a tapered wing with twist, see Figure 22. However, as the tolerances are tightened it primarily optimizes twist to increase the angle of attack while the chord is optimized for the lift distribution with minimal help from twist to minimize drag.

As I was implementing each variable of the design space I noticed that the last variable I implemented, twist, slowed down the optimization significantly and with little benefit. I then opted to rerun the optimization with the same variables but optimizing span instead of twist and span instead of chord. The wing and plane optimized for span and chord resulted in essentially one solution, this solution varied across the ten starts with varying dihedral angles. A front view of these airframes can be seen in Figure 23. The chord distribution and rest of the airframe were essentially the same but did vary slightly to adjust accordingly for the dihedral. I had to adjust the limits of this optimization to allow the tail to be moved further back. Prior to this adjustment the optimized airframes had the tail positioned just above the wing as it greatly reduced the span, greatly lengthened the chord, and this arrangement yielded a poor optimized goal value. This issue went away by allowing the tail to move five more meters back. Interestingly enough they all had essentially the same root chord and span. An example of the chords and airframe of the the design can be seen in Figures 24 and 25, as mentioned these vary slightly by design but not by enough to be noticed in a figure.

When optimizing span instead of chord distribution the optimizer failed to converge to a feasible solution. Using multi-start it hit several infeasabilities or breakdowns in the problem after many iterations for each starting point. This left us with the two solutions; one that was optimized for all the common variables and span, the other for the same common variables and twist. The one optimized for twist instead of span had a slightly better optimized goal parameter and used less material in the wings and fuselage. While slightly more complicated to manufacture with twist it offers a significant performance and material cost advantage to be the optimal design for this problem. Each solution is outlined in detail in Table 3.
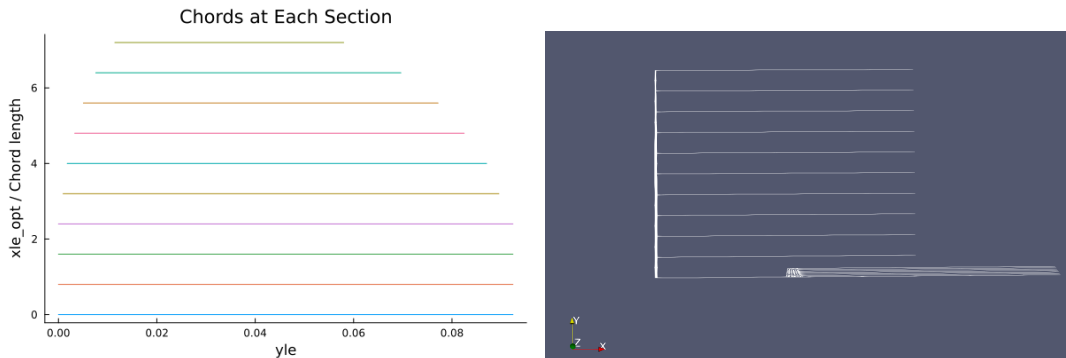

Figure 20: The wing chord distribution of the optimized airframe

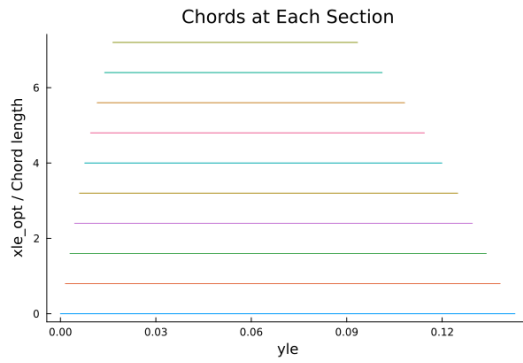Figure 21: An overhead view of the optimized airframe

Figure 22: Preconverged tapered wing solution

Figure 23: Front view of airframe optimized for chord and span
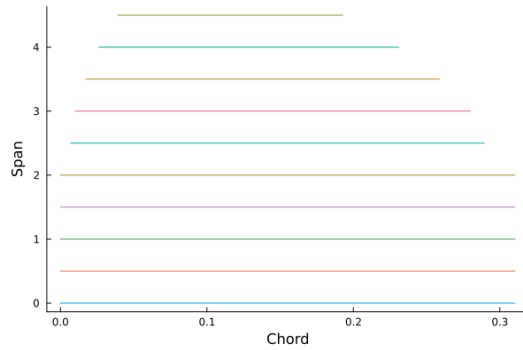

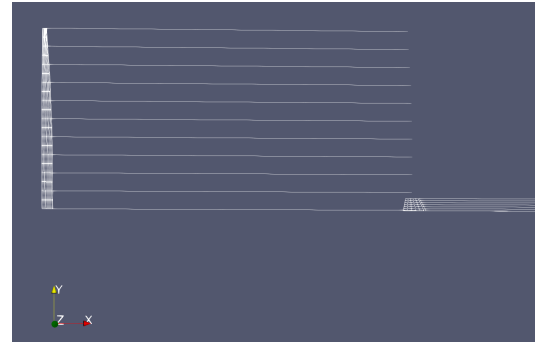Figure 24: Wing of airframe optimized for chord and span

Figure 25: Overhead view of airframe optimized for chord and span

6 Conclusion

This course has provided me the tools to analyze, design, and optimize aircraft for various aerodynamic measures. It has provided me with the context to interpret and understand those problems and the optimized result. It has also helped me in understanding how to formulate and set up those optimization problems. These are valuable tools in tackling the design space of complex mechanical machines such as aircraft structures. The final objective I settled on was range as it relates to the utilitarian performance of an airframe in total, constrained for stability. The final design selected optimized for chord length, the number of wing sections, twist, dihedral of the wings, flight speed, position of the tail, the length of the vertical stabilizer, and the length of the horizontal stabilizer for performance and manufacturability.

Table 3: Final 2 optimized designs

	Optimized Design 1	Optimized Design 2
Span (m)	Constrained to 16	9
Dihedral (degrees)	5	2.71
Flight Speed (m/s)	10	10
Horizontal Tail Size (m)	0.326	0.339
Vertical Tail Size (m)	0.077	0.077
Tail Position (m)	5	10
Twist (degrees)	0.006	0
Chords (m)	0.092, 0.092, 0.092, 0.092, 0.089, 0.085, 0.079, 0.072, 0.062, 0.047, 0.035	Constrained to 1
Optimized Multiplier	349.63	194.07

References

[AB94] David N. Anderson and Daryl L. Bonhaus. Simplified aerodynamic analysis of slender delta
        wings with leading-edge vortex flows. Technical report, NASA Technical Memorandum 110419,
        1994. Accessed: 2024-09-10.

[Aer24] AeroToolbox. Lift, drag, and moment coefficient. 2024. Accessed: 2024-09-10.

A   Appendix A

Table 4: Effect of tail volume on pitch and yaw stability derivatives

					Vh												
				0.875					3.0625					5.25			
			α	β	p	q	r	α	β	p	q	r	α	β	p	q	r
Vv	0.028	Pitch	-1.20	1.08	-0.21	-22.62	-0.05	-6.57	3.94	-1.51	-296.70	-2.70	-11.88	6.70	-2.80	-881.53	-4.83
		Yaw	0.00	0.06	0.00	0.00	-0.67	0.00	0.06	0.00	0.00	-0.05	0.00	0.06	0.00	0.00	-0.05
	0.168	Pitch	-1.20	0.30	-0.21	-22.62	-0.05	-6.57	0.67	-1.51	-296.70	-0.06	-11.88	6.04	-4.56	-881.53	-24.14
		Yaw	0.00	0.39	-0.13	0.00	-1.88	0.00	0.39	-0.13	0.00	-1.88	0.00	0.40	-0.13	0.00	-1.93
	0.308	Pitch	-1.20	0.30	-0.21	-22.62	-0.05	-6.57	0.67	-1.51	-296.70	-0.06	-11.88	1.05	-2.81	-881.53	-0.25
		Yaw	0.00	0.72	-0.48	0.00	-6.36	0.00	0.72	-0.48	0.00	-6.36	0.00	0.72	-0.48	0.00	-6.36